Polarization properties of quasielastic light scattering in fused-silica optical fiber

S. H. Perlmutter, M. D. Levenson, and R. M. Shelby
IBM Research Division, Almaden Research Center, 650 Harry Road, San Jose, California 95120-6099

M. B. Weissman
Department of Physics, University of Illinois at Urbana-Champaign, 1110 West Green Street, Urbana, Illinois 61801
(Received 11 December 1989)

Polarized and depolarized components of the quasielastic light-scattering spectrum of fused-silica optical fiber have been measured in the frequency range 100 kHz to 100 MHz at temperatures from 10 to 293 K. The depolarization ratio was found to be 0.14 ± 0.03. In the backscattering geometry both polarization components are seen to obey an inverse-power-law frequency dependence. Both the temperature and frequency dependence are consistent with a model that assumes thermal activation of structural relaxations which have a wide distribution of relaxation-time constants. In the forward direction, an additional polarized component with the same temperature dependence appeared.

INTRODUCTION

Amorphous materials have several categories of ubiquitous but poorly characterized structural fluctuations.[1] In the subkelvin regime, heat-capacity, thermal-conductivity, and acoustic-absorption measurements in a variety of materials indicate the presence of localized nonharmonic modes, usually assumed to be two-level systems (TLS's).[2] At higher temperatures, acoustic measurements, dielectric dispersion,[1] neutron scattering,[3] electrical noise,[4] and quasielastic light scattering[5,6] (QELS) also indicate, in various amorphous materials, the presence of structural fluctuations. These fluctuations typically have thermally activated kinetics above about 20 K.[1,7] In the subkelvin regime, tunneling kinetics are dominant.[2,7,8] Despite general agreement on these qualitative features, a number of basic questions remain to be answered about the fluctuations in even the best-studied amorphous materials, such as amorphous silica (a-SiO_2).

It is not known in general whether the subkelvin properties and the thermally activated fluctuations both result from essentially similar double-well systems (DWS's). Furthermore, in most materials no specific pictures for such DWS's have been developed, although a suggestion has been made for a-SiO_2,[3] and there is a reasonable model for a rather special case—the orientational glass $(KBr)_{1-x}$ $(KCN)_x$.[9] In fact, it is not generally known whether the fluctuations within the activated regime in any one material are well described by a single type of structural picture.

The distribution of level splittings of the structural fluctuations has been accurately measured in many materials, including a-SiO_2, in the tunneling regime below 1K, where these modes make a major contribution to the heat capacity.[2] However, at higher temperatures there has been little quantitative information on the relevant distributions of DWS parameters. An approximately constant density of states is known to fit ultrasonic attenuation[10] and quasielastic-neutron-scattering[3] data better than a distribution with some maximum splitting of less than ~ 300 K, but these previous data have not provided accurate enough information on the frequency dependence of the spectral density to cleanly separate density-of-states effects from kinetic effects.

One way to check whether all of these effects have a single physical origin (or result from a collection of dissimilar modes) is to measure several fluctuating quantities in a single frequency range in a particular glass as a function of temperature. Such experimentally measurable quantities include polarizability tensor fluctuations (studied via polarized and depolarized QELS), strain-tensor fluctuations (studied via ultrasound absorption or internal friction), and electric polarization (probed via dielectric loss). If a number of such measurements closely track each other, it becomes increasingly reasonable to look for a single characteristic fluctuation structure. For example, ultrasound absorption and dielectric dissipation often show similar temperature dependences in the activated regime, strongly indicating that both come from the same sites.[1] However below about 40 K, dielectric loss is much less temperature dependent than acoustic loss, indicating that a new set of low-energy, low-barrier-height fluctuations with relatively large electric-dipole to elastic-dipole ratios must be active.[1]

With the exception of this series of experiments, previous light-scattering studies of glasses,[6,11] including a-SiO_2, have employed standard Fabry-Perot or grating-spectrometer methods for resolving frequency shifts, and thus have been limited to frequencies above about 100 GHz. In that frequency range, components other than those due to structural fluctuations are also present, complicating the data analysis. In particular, such experiments have not resolved the line shape of the light-scattering component due to structural fluctuations. They have, however, demonstrated that a QELS component apparently due to structural fluctuations is present in a variety of glasses. Furthermore, ratios of

depolarized to polarized QELS have been obtained for many glasses, although not as a function of temperature.[5]

We have reported in an earlier paper[12] the observation of quasielastic light scattering in fused-silica optical fiber with an inverse-power-law frequency dependence ($1/f$ QELS). Here we report an extensive series of similar homodyne-detected light-scattering experiments in which we observed polarized and depolarized components of $1/f$ QELS, and a large polarized QELS signal in forward-scattered light at MHz frequency shifts and at temperatures down to 10 K. Both previous[12] and present $1/f$ QELS data are well described by a modified Dutta-Horn (MDH) model[4,12,13] based on the physically reasonable assumption of a distribution of structural-relaxation-time constants in glass. Three of the main goals of the homodyne QELS experiments reported here concern characterization of the structural fluctuations. First, by combining accurate spectral data over a wide temperature range, we determine distributions of activation energies and of level splittings in three slightly different glasses: pure fused silica, germania-doped silica, and stressed germania-doped silica. Second, by measuring the depolarization ratio over a wide temperature range, we have determined that a single type of fluctuation appears to be dominant in a-SiO_2 of high purity. That conclusion is reinforced by an approximate comparison with acoustic measurements[1] on similar material. Third, by determining absolute levels of two fluctuation parameters, and by successful application of a modified Dutta-Horn model, we hope to provide input from which constraints on the structural model of the DWS's may be calculated.

LOW-FREQUENCY SCATTERING MECHANISMS IN FUSED-SILICA OPTICAL FIBER

The experiments described here used single-mode fused-silica optical fiber as the scattering medium which, although used extensively in telecommunications as a low-noise transmission line, is nonetheless a useful material with which to study light-scattering processes. Optical fibers consist of a ~ 125-μm cylindrical fiber of a dielectric material (typically fused silica) with a ~ 5-μm core of a dielectric with a higher refractive index (typically obtained by doping either the core or the cladding). Optical fibers are particularly useful for studying processes which scatter light only weakly, as they allow high-intensity incident light to be guided over long interaction lengths. Observation of four scattering mechanisms in fused-silica optical fiber have previously been reported: Raman scattering,[11] Brillouin scattering[14] [and guided-acoustic-wave Brillouin scattering[15] (GAWBS)], Rayleigh scattering, and $1/f$ quasielastic light scattering.[12] In addition, a dynamical central scattering peak was first observed in a glass by Firstein, Cherlow, and Hellworth in 1975.[16] Since then, this central-peak scattering has been investigated extensively as a direct way of studying two-level tunneling systems and thermally activated structural relaxations in glass.[3,6] The $1/f$ QELS recently observed was not identified in previous experiments due to the lack of sufficient resolution or sensitivity at low frequencies (below 100 MHz).

Conventional Brillouin scattering in an optical fiber produces a component shifted by >20 GHz in the backscattering geometry and essentially no forward scattering. Our apparatus is insensitive to the spontaneous Brillouin scattering, and we scrupulously avoid conditions leading to stimulated Brillouin scattering. Thermally excited vibrations of the cylindrical fiber modulate the density of the core and hence its refractive index, creating phase noise. This guided-acoustic-wave Brillouin scattering, or GAWBS, can be detected in the forward direction even in 1 m of fiber.[15] Figure 1 shows four low-order modes of these mechanical vibrations. Modes which are cylindrically symmetric have no effect on the polarization of scattered light. However, modes with planes of symmetry along orthogonal diameters induce birefringence in the fiber and depolarize scattered light. Both types of modes can be explored using variations of our forward-scattering homodyne-detection technique. Figure 2 shows part of the GAWBS spectrum for 100 m of single-mode fused-silica optical fiber at room temperature along with the quantum-noise level. The spectrum is highly structured; each peak corresponds to a mechanical resonance of the fiber with kT of energy in each mode. The peaks are broadened by damping due either to the acoustic attenuation of the glass itself or to the jacket material which covers most fibers. Inhomogeneities in the fiber diameter also contribute to the broadening of the resonant peaks. The spectral structure is well modeled as described in Ref. 15.

Rayleigh scattering, caused by dynamic inhomogeneities due to temperature-entropy fluctuations, has also been observed in fused silica.[12] As shown in Fig. 3, Rayleigh scattering appears in our homodyne-detected

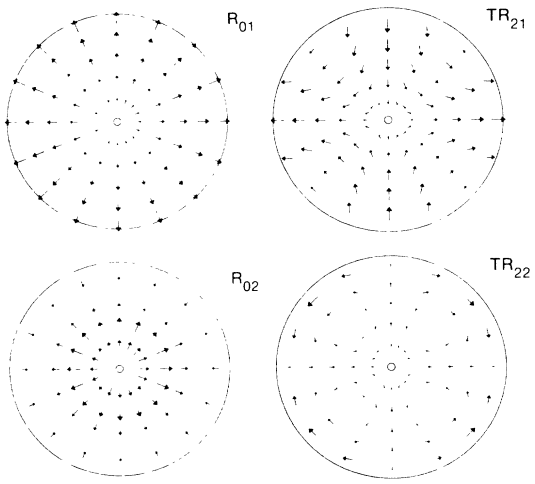

FIG. 1. Cross section of an optical fiber showing the four lowest-order mechanical vibration modes of each symmetry: radial modes R_{01} and R_{02} and mixed torsional/radial modes TR_{21} and TR_{22}. Cross sections on the left indicate cylindrically symmetric modes which uniformly stress the fiber's core (through which the light propagates) and do not induce birefringence in the fiber. Cross sections on the right indicate modes responsible for depolarized GAWBS (Ref. 15).

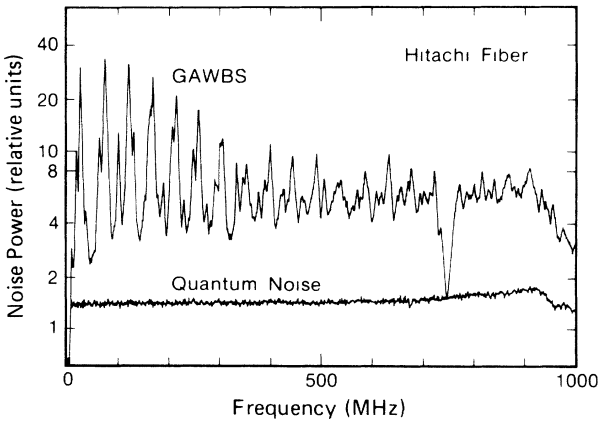

FIG. 2. GAWBS spectrum over a 1-GHz bandwidth. The dip down to the quantum-noise level corresponds to the first resonance of the phase-shifting optical cavity used in making homodyne measurements of the phase noise (Ref. 15).

backscattering spectra as a broad ($\sim$150-MHz-wide) Lorentzian which dominates all other low-frequency scattering features at room temperature.

An additional component of quasielastic light scattering in glasses has been attributed to thermally activated structural fluctuations. This component has been resolved spectrally in SiO_2 fibers and was shown to have a frequency dependence that obeyed an inverse power law.[12] This $1/f$ peak also contributes a low-frequency slope in Fig. 3. Thermally activated structural fluctuations also give rise to ultrasound absorption,[1] dielectric loss,[1] and inelastic neutron scattering.[3] The peak in the QELS signal as a function of temperature corresponded to the temperature of the maximum expected from these

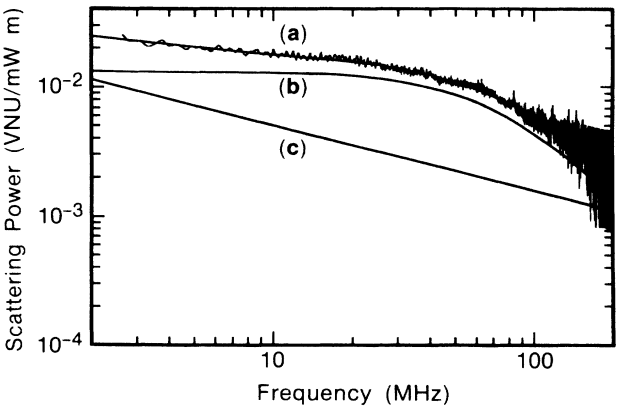

FIG. 3. (a) Room-temperature Rayleigh scattering in germania-doped low-birefringence fused-silica optical fiber. The measured spectrum has two components: a 139-MHz-FWHM-wide Lorentzian due to dynamic Rayleigh scattering and a $1/f$ QELS component with a frequency exponent of 0.5. The two solid lines below the spectrum show (b) the isolated Rayleigh and (c) the $1/f$ QELS components. The spectrum is in vacuum-noise units (VNU's) per milliwatt of optical power coupled into the fiber per meter of fiber length, and agrees with theoretical expectations.

other experiments. However, the previous measurements of QELS in a-SiO_2 were insensitive to the depolarization ratio of the scattering process.

EXPERIMENT

Three experimental configurations were used. All used homodyne detection of the scattered light. A discussion of homodyne detection and our method of data reduction appears as an appendix to this paper.

The first experimental configuration used a polarization-preserving fiber (a York V.S.O.P., Inc. fiber, type HB600), and was able to measure polarized and depolarized scattering signals independently. A diagram of this experimental configuration appears in Fig. 4. The refractive index of the core of the fiber was elevated by germania doping. The polarization preserving properties of the fiber were achieved by stressing the glass to induce high birefringence in the core, thus establishing two polarization eigenmodes in the fiber. A beam from a stabilized krypton-ion laser running on the 647.1-nm line was coupled through a 19-cm length of single-mode polarization-preserving fiber. This short length of fiber acted as a spatial filter and was cut from the longer fiber that acted as our scattering medium. Consequently, the transverse spatial mode of the incident beam after the spatial filter matched that of the longer fiber, resulting in good mode overlap of signal, pump, and local oscillator beams and high detection-system-homodyne efficiency.

After passing through the spatial filter, 25% of the power was split off and coupled into the "back" end of the fiber through polarization beam splitter C with polarization crossed with the incident (pump) beam. The remaining beam was passed through a Faraday optical isolator and coupled into the "front" end of the fiber. Roughly 4% of the light incident on the front face of the fiber was reflected and rejected, along with the polarized backscattered light, by polarizer A of Fig. 4. The light reflected from the input face acted as a local oscillator to allow the homodyne detection of backscattered polarized QELS excited by the forward-propagating pump beam. The "back" face of the fiber was bathed in refractive-

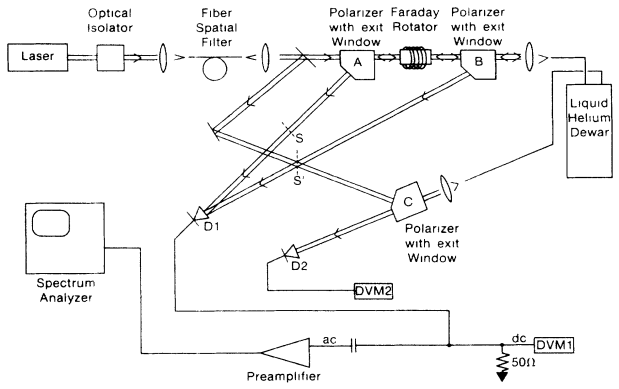

FIG. 4. Experimental apparatus for measuring polarized and depolarized backscattering. See the main text for a complete description.

index-matching oil to suppress its reflections. The beam propagating backward through the fiber acted as a local oscillator for depolarized scattering and, along with the depolarized scattered light, was rejected by polarizer B of Fig. 4. Blocking either polarizer A by closing shutter S, or B by closing shutter S', allowed only the depolarized or polarized backscattered light, respectively, to be measured. The scattered light and local oscillator beam beat on the face of FND-100 photodiode D1. The dc current produced by the photodiode generated a voltage on a 50-Ω resistor, which was measured by a digital voltmeter. The ac components were amplified with a custom low-frequency, low-noise, high-gain preamplifier. The gain was made to drop off 50 dB/decade below 100 KHz to prevent amplifier saturation. The homodyne signal was then displayed on a Hewlett-Packard model 8568 rf spectrum analyzer.

The fiber itself (143.5 m) was wound around an oxygen-free high-conductance (OFHC) copper drum, 3 in. in diameter and 10 in. in length, and mounted in a variable-temperature liquid-helium Janis dewar, model 10 CNDT. Silicon-diode temperature sensors were fastened to either end of the drum. Except during periods of rapid cooling, the temperature difference between the two sensors was within 0.2 K. A third sensor acted to maintain the temperature of the gas flowing through a capillary tube from the helium reservoir to the sample chamber at the set point. The attenuation of the fiber wound on the drum did not vary with temperature.

The homodyne beat signal of the polarized and depolarized scattering was measured over a range of temperatures. At each temperature, in addition to spectra of the homodyne-scattering beat signal, we also recorded spectra of the quantum-noise level and the dark- (electronic) noise level. The quantum-noise level was obtained by shining an incandescent lamp, covered by an ir rejection filter, into photodiode D1 at an intensity such that the photocurrent was the same as produced by the local oscillator beam during the actual experiment[17] (see Appendix). The dark-noise level was obtained by blocking all light into the photodiode. In data analysis, dark noise was subtracted from the raw-signal spectra, which were then normalized to the vacuum noise by dividing by the quantum-noise spectrum. This normalization procedure also corrected for moderate frequency dependence of the detector and amplifier response. The contribution of the vacuum noise was then removed by subtracting 1 from the normalized spectrum, yielding an absolute light-scattering spectral density in units (called "vacuum-noise units") of the vacuum-noise spectral density (equal to one-half quantum per unit of spectrum-analyzer bandwidth).

The scattering efficiency per meter was then obtained by dividing the corrected and normalized scattering spectral density by the incident pump intensity measured by detector D2, the length of the optical fiber, and by the overall detection efficiency (see Appendix). The detection efficiency was limited primarily by the transverse-mode overlap of the scattering and local oscillator beams and was measured independently.

In addition to the polarized and depolarized backscattering, it was possible to obtain a homodyne signal of depolarized forward scattering by using the apparatus diagramed in Fig. 5. The fiber was not perfectly polarization preserving. Indeed, at temperatures below ~ 150 K the polarization of the incident beam in the fiber would wander, putting up to 10% of the optical power into the cross polarization. Therefore, the light incident on detector D1 from polarizer C in Fig. 5 contained not only the forward depolarized scattering, but also up to 10% of the incident beam, which then served as a local oscillator for homodyne detection. Scattering spectra were recorded only when the polarization in the fiber wandered slowly compared to the time necessary to make the measurement.

The third experimental configuration used a random birefringence fiber (Hughes Research pure-silica 5-μm core with a numerical aperture of 5.26×10^{-3}) which did not preserve polarization. This experimental apparatus, which detected only forward-scattering light, appears in Fig. 6.[17,18] A stabilized single-frequency 647.1-nm krypton-ion laser beam was coupled into 114 m of single-mode fused-silica optical fiber with its jacket removed and installed in a variable-temperature liquid-helium Dewar. The looped fiber hung freely in the Dewar. A silicon-diode temperature sensor hung freely within the loop of fiber.

The output beam from the fiber was reflected from a confocal Fabry-Perot cavity with axial-mode spacings of approximately 748 MHz and a finesse of approximately 35. This cavity was resonant for the incident 647.1-nm pump wave and served to phase-shift this beam relative to the scattered light which was frequency shifted from the pump by more than the cavity linewidth (approximately 20 MHz). In this way, forward-scattered light, due to GAWBS and other QELS processes, which was originally in quadrature relative to the incident beam, was made to be in phase with the reflected beam, which then acted as a local oscillator, allowing homodyne detection of the scattered-light signal. The data were reduced

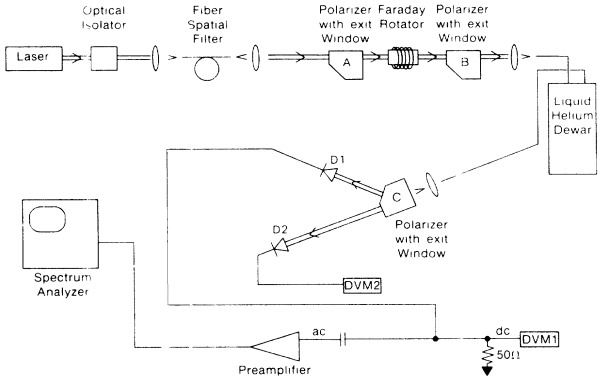

FIG. 5. Experimental apparatus for measuring depolarized forward scattering. The depolarized forward-scattered light is rejected by polarizer C. In addition, up to 10% of the pump "leaks" into the cross-polarization and is also rejected by polarizer C. This pump light serves as a local oscillator for homodyne detection and beats with the depolarized forward scattering.

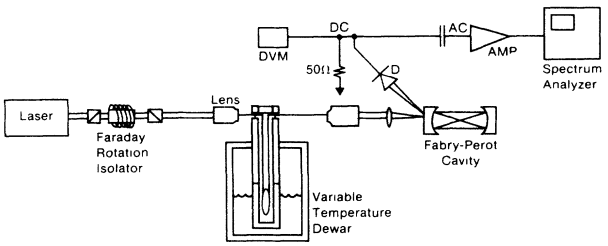

FIG. 6. Experimental apparatus for measuring forward scattering in a non-polarization-preserving fiber. Light from a single-mode krypton-ion laser is coupled into a single-mode optical fiber. After propagating through the fiber (which was installed in a variable-temperature liquid-helium Dewar), the beam was put into a phase-sensitive homodyne-detection system consisting of a phase-shifting optical cavity, used to convert phase noise to amplitude noise, and a broadband photodetector. The digital voltmeter (DVM) recorded the local oscillator power.

as described above, except that the transmitted pump power had to be measured subsequently.

RESULTS

Figure 7 shows polarized and depolarized backscattering signals taken with the first of our experimental setups. The figure consists of multiple overlapping spectrum analyzer traces taken with different resolution bandwidths over a variety of frequencies intervals. Our normalization procedure results in near-perfect overlap. Figures 7(a) and 7(b) show polarized (p) and depolarized (d) backscattering at room temperature and 84.2 K, respectively. At the colder temperature the spectral line shapes clearly obey an inverse power law over three decades of frequency bandwidth, with the depolarized scattering 0.14 times the polarized. At room temperature, the depolarized scattering shows clear $1/f$ behavior below 500 kHz. Above this frequency the strength of scattering due to other thermally excited mechanisms becomes comparable to the $1/f$ QELS component. The line shape of the polarized scattering spectrum is similar to the total (both polarized and depolarized) backscattering spectrum at room temperature of the germania-doped random-birefringence fiber shown in Fig. 3. This spectral line shape can be fitted well by a superposition of a Lorentzian and an inverse-power-law spectrum. The Lorentzian's amplitude and linewidth are consistent with predictions for the conventional (dynamic) Rayleigh line of fused silica.[19,20]

At frequencies below 75 kHz, microphonic pickup by the fiber and laser cavity created an intermittent noise level which precluded reliable measurement of the light scattering.[21] The limited bandwidth of our present low-noise preamplifier and the decreasing $1/f$ signal at higher frequencies limited the bandwidth of absolute measurements to below 100 MHz.

The temperature dependence of the polarized and depolarized scattering efficiencies at 1 MHz is shown in Fig. 8 and is similar to that reported earlier for a non-polarization-preserving fiber. The depolarized data include points from both forward and backward depolarized scattering. In general, spectra of these two scatter-

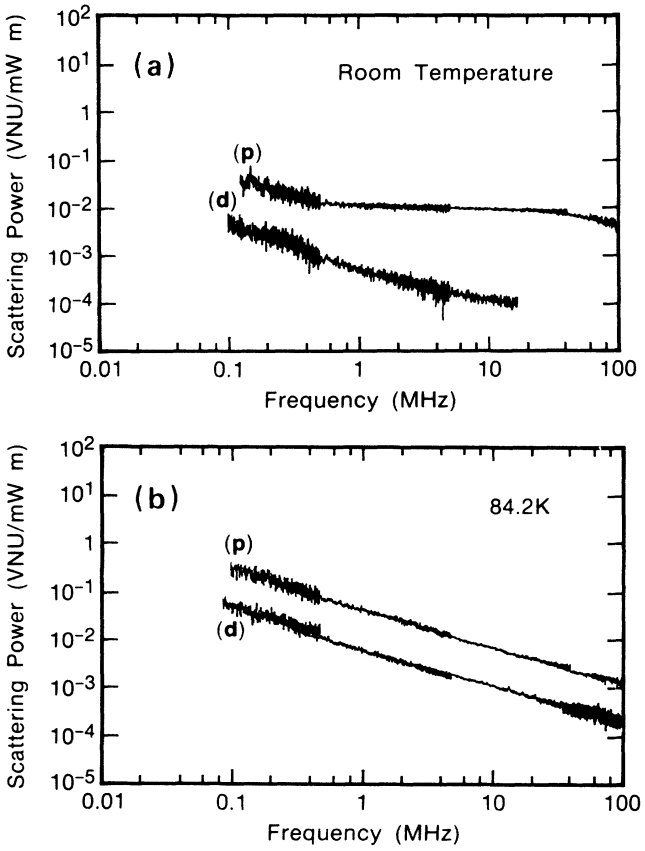

FIG. 7. (a) Homodyne-detected polarized (p) and depolarized (d) backscattering at room temperature. The polarized signal is dominated by Rayleigh scattering, while $1/f$ QELS behavior is clearly visible in the depolarized signal. The scattered power is measured in vacuum-noise units (VNU's) at the photodetector and normalized with respect to laser power coupled into the fiber and the fiber length. (b) Homodyne-detected polarized (p) and depolarized (d) backscattering at 84.2 K. Both polarized and depolarized scattering signals show $1/f$ behavior for over three decades of frequency.

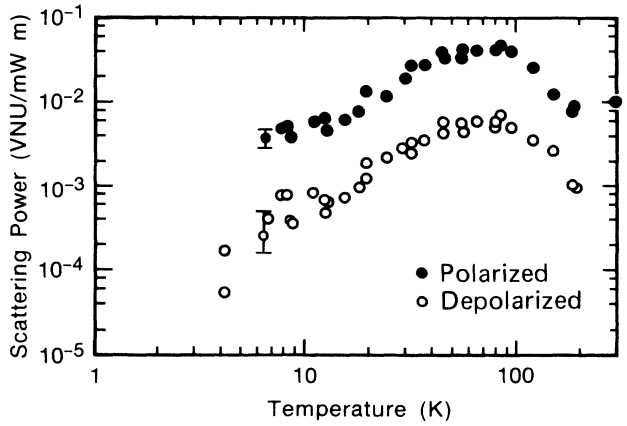

FIG. 8. Temperature variation of both polarized and depolarized scattering power at 1 MHz. The spectra are shown in units of vacuum noise per mW of power coupled into the fiber per meter of fiber length. Typical error brackets are shown for low temperatures, where experimental uncertainties are most significant. Above 20 K the error bars are the size of the circles.

ing geometries agreed well. That the temperature dependence of both the polarized and depolarized scattering track each other so well indicates that it is likely that both arise from the same structural fluctuations. This sort of temperature dependence is also similar to that measured for the ultrasound absorption in fused silica, which has been interpreted in terms of interactions with double-well systems.[1,10] The ~80-K peak in the 1-MHz structural fluctuations found by light scattering coincides well with the peaks found via ultrasound absorption and dielectric dispersion,[1,22,23] when one multiples the latter two dissipation parameters by T to convert to fluctuation magnitude. A comparison of light-scattering data and appropriately adjusted ultrasound absorption data[1] (Fig. 9) shows similar temperature dependencies. It is reasonable to presume that these two effects (and dielectric dispersion) come from the same transitions, at least in this temperature range.

Figure 10 shows several typical spectra of forward scattering obtained using the third of our experimental set ups (Fig. 6) at three different temperatures. The peaks correspond to GAWBS modes of the pure-silica core fiber.[15,18] As each GAWBS mode is excited by kT of energy, the area under each peak would be expected to decrease linearly with temperature. Spectra of forward scattering at 295, 100, and 2 K are shown in Fig. 10 as traces (a), (b), and (c), respectively. Note how the GAWBS peaks fall monotonically with temperature, while the background level between the peaks is highest in the 110-K spectrum. Several peaks do not change height at all with temperature. These peaks are due primarily to the unstripped ends of the fiber which come out of the Dewar and are at room temperature at all times. Figure 11 shows the peak heights of various frequency components as a function of temperature. Between 293 and 80 K, the GAWBS peak at 49.6 MHz is seen to fall slightly faster than linearly and slightly slower between 80 and 20 K. This variation from linear behavior could be due to a temperature-dependent ultrasound absorption which peaks near 80 K, but the variation in peak height

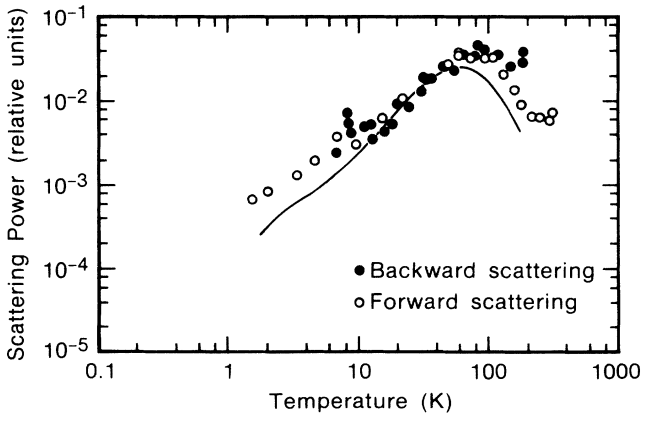

FIG. 9. Comparison of forward- and backward-polarized $1/f$ QELS (circles) with ultrasound-attenuation data (in units of inverse mean free path) which has been adjusted by multiplication by temperature (solid line).

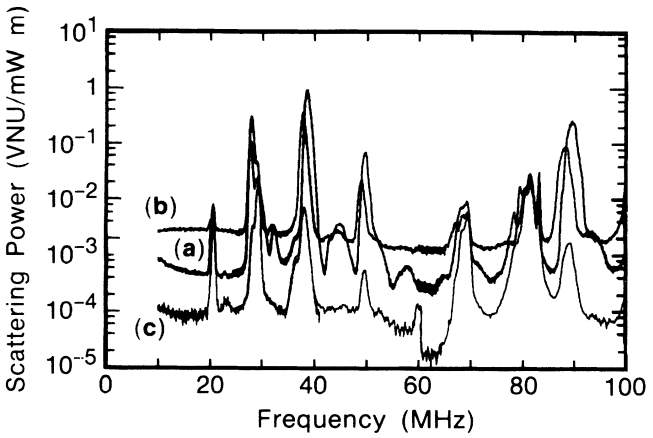

FIG. 10. Forward-polarized scattering from a pure-fused-silica-core fiber at (a) room temperature, (b) 110 K, and (c) 2 K. The spectra are dominated by GAWBS peaks which arise due to thermally excited mechanical resonances of the bulk fiber. The background level is seen to rise initially upon cooling, reaching a maximum height at 80 K before falling with continued cooling.

basically confirms expectations for a harmonic-phonon mode in thermal equilibrium. Damping of GAWBS resonances due to ultrasonic absorption causes broadening of the resonance linewidth, reducing the peak height at temperatures where the damping is greatest.

Although the spectrum of other scattering mechanisms cannot be isolated from that of GAWBS in Fig. 10, the region of the spectrum between GAWBS peaks, i.e., at 11, 55, and 98 MHz, has a temperature dependence remarkably similar to that of the $1/f$ QELS seen in the backward direction (Fig. 8). However, the strength of this scattering signal does not have a systematic frequency dependence. The scattering-efficiency–versus–temperature curve at 98 MHz looks nearly identical both

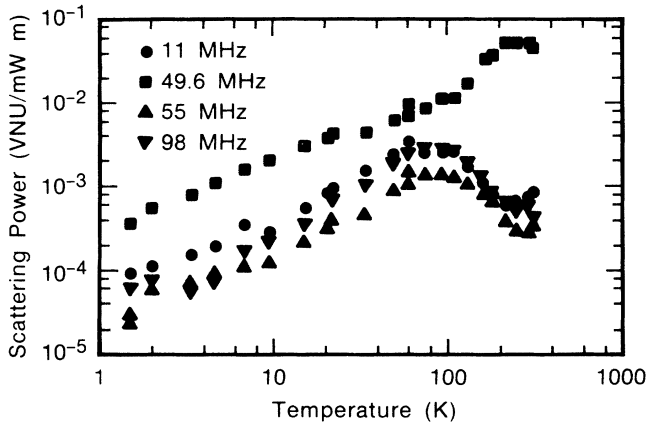

FIG. 11. Temperature variation of the height of the GAWBS peak at 49.6 MHz and the background level between GAWBS peaks at three different frequencies. The deviation from a linear dependence of the GAWBS peak height on temperature may be due to temperature-dependent acoustic attenuation (and linewidth), which peaks at 80 K. The temperature variation of the background scattering level between GAWBS peaks is similar to that of the backwards scattering.

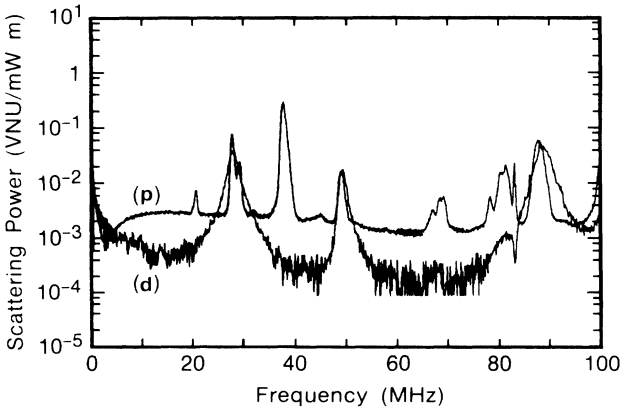

FIG. 12. Scattering efficiency of polarized and depolarized forward scattering. The background level of the depolarized spectrum is a factor of 0.13±0.01 times the polarized background.

in shape and absolute amplitude to the corresponding curves at both 11 and 55 MHz. It is possible that this scattering may be due to an interaction between the DWS responsible for $1/f$ QELS and the phonons producing GAWBS, but no model has been developed to support this conjecture.

Figure 12 shows the scattering efficiency of polarized and depolarized scattering in the same fiber in the forward direction at 77 K. The depolarized GAWBS peaks have very nearly equal magnitude in both spectra. However, the background level of the depolarized spectrum is a factor of 0.13±0.01 times the polarized background. A $1/f$ component is visible in the depolarized spectrum, but the apparatus needed for the polarized spectrum did not function below ~7 MHz. One must also note that the polarized background cannot be attributed to wings of the Lorentzian GAWBS lines. This depolarization ratio for the background is similar to the corresponding ratio for backward-scattered light.

The temperature dependence of the frequency exponent of the power-law $[\eta(\omega)\propto\omega^{-\alpha}]$ light-scattering efficiency is shown in Fig. 13. Although the scattering

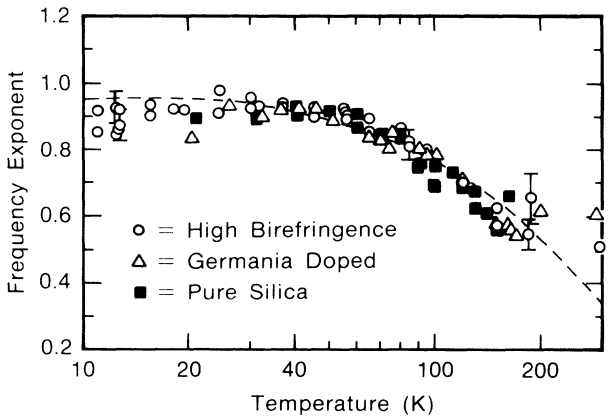

FIG. 13. Temperature variation of the frequency exponent α of the scattered power for three fibers. The exponent was found to be constant from 0.1 to 100 MHz. The dashed line is a prediction using the modified Dutta-Horn equation, Eq. (7), and the 1-MHz data in Fig. 8.

power was shown in Fig. 8 to depend on whether the scattering is polarized or depolarized, it appears that the frequency exponent and temperature variation do not. Figure 13 includes data obtained from polarized and depolarized backscattering as well as forward depolarized scattering. The data from all three scattering geometries agree well. Also included in Fig. 13 are frequency-exponent data from backscattering experiments done with non-polarization-preserving fibers with cores of pure a-SiO_2 and germania-doped a-SiO_2. The agreement in data from all three types of fibers suggests that $\alpha(T)$ may be insensitive to composition, unlike the absolute scattering level.

DISCUSSION

Power-law frequency spectra often can be modeled by assuming that they arise from a collection of DWS's, each of which contributes a Lorentzian spectrum[4]

$$S(\omega)\propto\frac{\tau}{1+\omega^2\tau^2}\ . \tag{1}$$

Taking $D_1(\tau)$ to be the probability density function of τ, the net spectrum is given by

$$S(\omega)\propto\int\frac{\tau}{1+\omega^2\tau^2}D_1(\tau)d\tau\ . \tag{2}$$

When the transitions of the DWS's are thermally activated, τ is given by $\tau=\tau_0\exp(E_a/kT)$, where τ_0 is a characteristic attempt time, typically of order 10^{-13} s, and E_a is the activation energy. E_a and τ_0 can each have a distribution of values contributing to a distribution of τ, but when the observed frequencies are much less than 10^{12} Hz the distribution of E_a is usually much more important, due to the exponential factor, so that τ_0 can be treated as a constant.

If we assume that the same DWS's are active at all temperatures, we obtain

$$S(\omega,T)\propto\int\frac{\tau_0\exp(E_a/kT)}{1+\omega^2\tau_0^2\exp(2E_a/kT)}D(E_a)dE_a\ . \tag{3}$$

As long as $D(E_a)$, the probability density function of E_a, varies slowly compared with kT, the integrand is dominated by values of $\tilde{E}\simeq -kT\ln(\omega\tau_0)$, allowing $D(\tilde{E})$ to be pulled outside the integral in Eq. (3). The integral can then be solved exactly, yielding

$$S(\omega,T)\propto\frac{kT}{\omega}D(\tilde{E})\ . \tag{4}$$

Both the T and ω dependencies of $S(\omega,T)$ are determined by the same activation-energy-distribution function. Differentiating Eq. (4) gives the Dutta-Horn equation,[4]

$$\alpha(\omega,T)=1-\frac{1}{\ln(\omega\tau_0)}\left[\frac{\partial\ln S(\omega,T)}{\partial\ln T}-1\right]\ , \tag{5}$$

where $\alpha\equiv-\partial\ln S/\partial\ln\omega$. This equation presumes that the same DWS's are active at each temperature, and thus it gives a term in the temperature derivative that is purely

kinetic, in that it simply involves shifts in the spectral shape as a function of temperature.

The combination of very accurate measurements of the spectral exponent with temperature-dependent magnitude data allows us to make an accurate determination of the nonkinetic factors entering into the quasielastic-scattering magnitude in the thermally activated regime. Such factors can be of two types. First, there is the simple thermodynamic factor resulting from the ability of states with larger level splittings E to fluctuate only at higher temperatures. The contribution of a DWS to the fluctuation spectrum is proportional to $\mathrm{sech}^2(E/2kT)$, where E is the level splitting. Thus only states with $E \leq 2kT$ contribute much. In the simplest form of the DWS picture, with a constant density of level splittings, this would give a factor of T in the QELS intensity. The low-temperature (below 1K) heat capacity, however, scales as $T^{1.3}$, indicating that the assumption of a constant density is not accurate in every regime.[2] A second possible temperature factor could result if the fluctuating sites had polarizability changes which were correlated with their level splittings. (Correlation of fluctuation size with activation energy, E_a, would appear in both the temperature dependence and the spectral slope, and would thus not affect their relation.) Since we have no indication in the depolarization ratio of any change in the properties of the fluctuating sites as a function of temperature, and since no other studies have indicated a need to consider such factors, we shall assume that all the deviations from the Dutta-Horn relation above about 20 K may be attributed to the distribution of level splittings.

Equation (5) does not, in fact, fit our data. The unsurprising conclusion is that an additional thermodynamic temperature dependence is also required. If we made the simplifying assumption that the density of states (i.e., of level splittings) has the simple form $E^{\beta-1}$, then, we find[13]

$$S(\omega,T) \propto \frac{kT^{1+\beta}}{\omega} D(\tilde{E}) \, . \tag{6}$$

In differential form, this leads to a modified Dutta-Horn equation,[13]

$$\alpha(\omega,T) = 1 - \frac{1}{\ln(\omega\tau_0)} \left[\frac{\partial \ln S(\omega,T)}{\partial \ln T} - (\beta+1) \right] . \tag{7}$$

We find that over the temperature range 20–160 K that the average deviation of the temperature dependence from the Dutta-Horn relation is a factor of $T^{1.3\pm0.3}$, i.e., $\beta = 1.3 \pm 0.3$. This implies a distribution of level splittings of $E^{0.3\pm0.3}$. A curve obtained from Eq. (7) using the measured temperature derivatives and $\beta = 1.3$ is compared with the measured values of α in Fig. 13. The agreement is quite good, although there are some small systematic residuals.

Given that a constant $\beta = 1.3$ produces a good fit, we are justified in solving Eq. (6) for $D(\tilde{E})$. The distribution of barrier heights can be determined by isolating $D(\tilde{E})$ in Eq. (6) and substituting in our measured scattering-power spectrum as well as the necessary experimental parameters. Plots of $D(\tilde{E})$ for both the polarized and the depolarized scattering mechanisms appear in Fig. 14(a), where the value of β has been taken to be 1.3. The plots are made up of many overlapping frequency spectra, only some of which are shown; each spectrum is taken at a different temperature. The solid curves were taken from actual normalized and corrected frequency spectra, which were adjusted according to Eq. (6). The shaded region represents the envelope of experimental uncertainty. The two distributions are seen to be exponentials with a depolarization ratio of 0.14 ± 0.03. Both curves have an inverse slope of approximately 450 ± 75 K. These curves closely resemble the form $\exp(-\tilde{E}/V_0)$, proposed by Gilroy and Philips with our value of $V_0/k = 450 \pm 75$ K in good agreement with the original suggestion of 470 K. The region of the polarized $D(\tilde{E})$ curve corresponding to fiber temperatures below 70 K is shown in Fig. 14(b). There appears to be a deviation from exponential behavior below $\tilde{E}/k = (200$ K). This deviation is most likely due to a breakdown of the modified Dutta-Horn equation, which assumes that relaxation processes are dominated by thermal activation. These lower values of $\tilde{E}$ correspond to fiber temperatures of ~ 15 K, and a

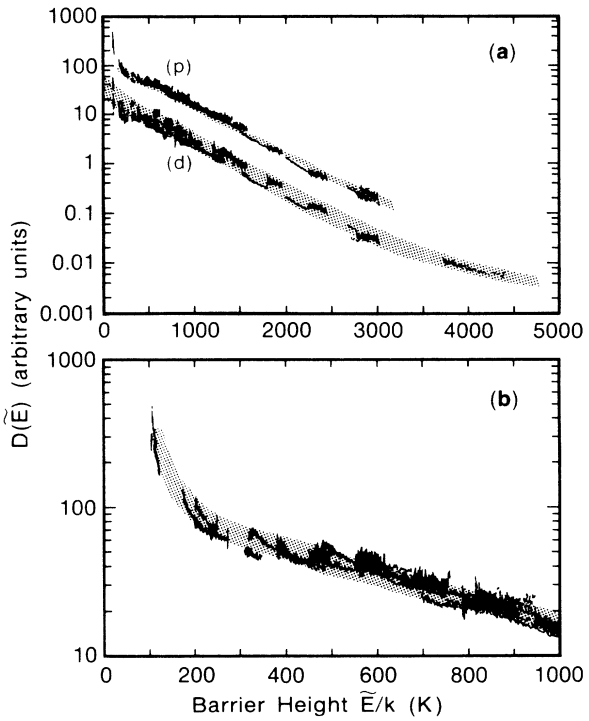

FIG. 14. (a) Experimentally inferred distribution of barrier heights of two-level systems in fused silica. The horizontal axis is in units of temperature. The individual lines correspond to polarized (p) and depolarized (d) scattering spectra like those of Fig. 7 taken at various temperatures which have been appropriately adjusted according to Eq. (6) in the text. The shaded regions represents the envelope of experimental uncertainty. The curves are well fitted by exponentials with inverse slopes of 450 K. (b) Region of the polarized $D(\tilde{E})$ curve corresponding to fiber temperatures below ~ 70 K. The constant determining the temperature scaling of the number of thermodynamically allowed thermally activated sites has been take as $\beta = 1.3$.

significant contribution of tunneling events to structural relaxation is likely.

A plot of $D(\tilde{E})$ for pure a-SiO_2 and germania-doped a-SiO_2 appears in Fig. 15. The Rayleigh-scattering component was subtracted from the spectra recorded at the higher temperatures. The Rayleigh component was determined by performing a least-squares fit of a superposition of an inverse power law and a Lorentzian spectrum to the measured scattering spectrum. The temperature dependence of the strength of the Rayleigh line determined in this way agreed well with theory.[19,20] Both these curves are also seen to be exponentials with inverse slopes of 407±40 K. In a previous paper,[12] the value of τ_0 was taken to be 10^{-12} s. With this value of τ_0 the inverse slopes of the curves in Fig. 15 were calculated to be 325 K (in Ref. 12 these were incorrectly reported as 290 K). Taking into account our assumption of τ_0 as 10^{-13} s, the current values are consistent with that of the previous paper.[12]

In the tunneling regime, the relaxation rate of a TLS is only weakly temperature dependent,[8] e.g., going as $\coth(E/2kT)$ in the single-phonon-relaxation regime. The dependence of the spectral density on temperature due to kinetics should be very weak in the tunneling regime, as long as the frequencies observed are well below the maximum rate for TLS's with energy splitting less than about $2kT$. In other amorphous materials in which it has been possible to distinguish between activated and tunneling kinetics,[7] tunneling kinetics usually become dominant below about 20 K, so that the Dutta-Horn relation becomes inapplicable. In the pure tunneling regime, at frequencies below the maximum tunneling rate, the temperature dependence of the spectral intensity should mainly reflect the number of fluctuating sites, i.e., the integral of the density of states. From 1.4 to 20 K the QELS intensity increases as about $T^{1.3}$, which agrees within experimental error with the extrapolated value from the low-temperature heat capacity.

It is interesting to note that the density of states appears to be a weakly increasing function of energy over the entire range of temperatures explored. The average temperature scaling of the number of active sites ($\beta=1.3$) is in surprising agreement with the subkelvin heat-capacity result.

At temperatures below 4.2 K, the fiber was immersed in liquid helium with the ambient pressure pumped below atmospheric. Under these conditions, new structure in the scattering spectra rose above the background level which had a clear inverse-power-law line shape. Figure 16 shows the forward depolarized light-scattering spectrum in flowing gas at 4.61 K (dashed spectrum) and in liquid at 3.4 K (solid spectrum). The solid line is an inverse-power-law fit to the higher-temperature spectrum with a frequency exponent of $\alpha=1.1$. The origin of this new spectral structure is not clear. One possibility is that it is due to mechanical resonances of the copper block around which the fiber is wrapped (similar to the GAWBS scattering discussed earlier).

The difference between our depolarization ratio in a-SiO_2, 0.14±0.03, and that found by Winterling,[11] 0.30±0.03, is rather striking. Although the frequency range of the measurements differs by about 5 orders of magnitude (~3 MHz versus ~300 GHz), neither experiment found a frequency dependence of the ratio. Both types of measurements might be subject to poorly understood artifacts—most notably that our homodyne technique requires comparing homodyne efficiences for two substantially different experimental arrangements. A more interesting possibility is that the depolarization ratio is a sensitive function of contaminants, with relatively little depolarized scattering resulting from displacements of high-symmetry SiO_4 tetrahedra. Winterling's low-wave-number depolarization-ratio data appear to have been taken from a Suprasil I sample, with relatively large OH concentrations enhancing the scattering. Whatever the explanation of the difference between our measured depolarization ratio and Winterling's may be, the relative values of the ratio measured at different temperatures are not sensitive to calibration errors.

The nearly constant value of the ratio of polarized to

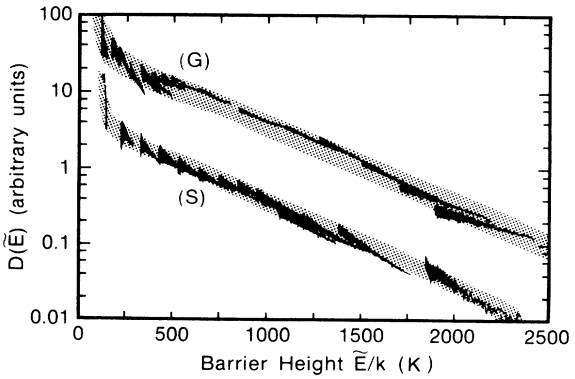

FIG. 15. $D(\tilde{E})$ for pure-fused-silica (S) and germania-doped fused-silica (G) fiber cores. Both curves are well fitted by exponentials with inverse slopes of 407 K. The constant determining the temperature scaling of the number of thermodynamically allowed thermally activated sites has been taken as $\beta=1.3$.

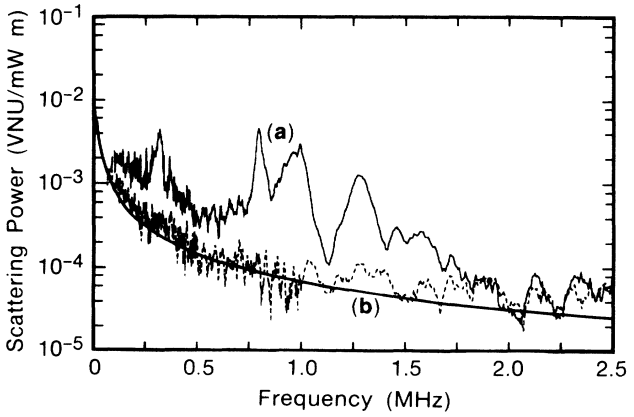

FIG. 16. Scattering power with fiber at (a) 3.4 K in liquid helium and at (b) 4.6 K in flowing helium gas. The solid line is an inverse-power-law fit to the higher-temperature spectrum, (b), with a frequency exponent of $\alpha=1.1$.

depolarized quasielastically scattered light over the temperature range 6–300 K gives important information about the structural fluctuations. The constancy of the ratio strongly suggests that the type of fluctuation causing both types of scattering is the same over the entire temperature range. There is no reason for different structural rearrangements to have so nearly equal ratios of scalar and traceless components of their polarizability changes.

Precisely what the structural fluctuations correspond to microscopically cannot, of course, be determined from a single ratio. A prediction for this depolarization ratio for any given model of the fluctuation is a worthy challenge to molecular-orbital theory. Such a prediction may then be compared with the measured value.

ACKNOWLEDGMENTS

This work was partially supported by the U.S. Office of Naval Research, and partially by the U.S. National Science Foundation under Grant No. DMR-86-17941.

APPENDIX: NORMALIZING HOMODYNE-DETECTED SIGNALS TO THE VACUUM-NOISE LEVEL

In homodyne detection the electric field at the photodetector responsible for photocurrent fluctuations at frequency δ has five components:

$$E(t)=\mathrm{Re}[E_{LO}e^{-i\omega t}+E_S(\delta)e^{-i(\omega-\delta)t}+E_A(\delta)e^{-i(\omega+\delta)t}+E_{VS}(\delta)e^{-i(\omega-\delta)t}+E_{VA}(\delta)e^{-i(\omega+\delta)t}] , \quad \text{(A1)}$$

where E_{LO} is the complex local-oscillator field and E_S and E_A are the complex stochastically fluctuating Stokes and anti-Stokes fields, respectively. The polarization state of this field is defined by the local oscillator, and the absolute phase is defined by the pump wave at the input to the fiber. E_{VS} and E_{VA}, the effective vacuum fields at the Stokes and anti-Stokes frequencies, respectively, will prove useful in providing a reference with which the absolute scattered power can be determined.

The photocurrent from the photodetector is proportional to the square of the total field amplitude,

$$|E(t)|^2\simeq|E_{LO}|^2+(E_{LO}E_S^*+E_{LO}^*E_A)e^{-i\delta t}+(E_{LO}^*E_S+E_{LO}E_A^*)e^{i\delta t}+(E_{LO}E_{VS}^\dagger+E_{LO}^*E_{VA})e^{-i\delta t}+(E_{LO}^*E_{VS}+E_{LO}E_{VA}^\dagger)e^{i\delta t} , \quad \text{(A2)}$$

where we have used the approximation $|E_{LO}|\gg|E_S|,|E_A||E_{VS}|,|E_{VA}|$ to eliminate insignificant terms.

It is useful at this point to define two quadrature amplitudes of the pump beam in terms of the Stokes and anti-Stokes fields. The amplitude and phase quadratures (responsible for amplitude modulation and phase modulation of the pump beam) can be written[18]

$$X_A=\frac{1}{\sqrt{2}}(E_Ae^{-i\theta}+E_S^*e^{i\theta}) , \quad \text{(A3a)}$$

$$X_\phi=\frac{-i}{\sqrt{2}}(E_Ae^{-i\theta}-E_S^*e^{i\theta}) , \quad \text{(A3b)}$$

where θ is the phase of the local oscillator relative to the phase of the pump, and it has been assumed that the pump and local oscillator are at the same optical frequency. It can be shown that forward-polarized light scattering from a thermally excited bath (as is QELS) results solely in phase modulation of the pump beam, i.e., forward-polarized scattering contributes only to the phase quadrature defined in Eq. (3b) above.[24] Therefore, we can set the amplitude quadrature, Eq. (3a), equal to zero. Solving Eqs. (3a) and (3b) for E_A and E_S^*, substituting into Eq. (2), and setting X_A equal to zero yields

$$|E(t)|^2=|E_{LO}|^2-\sqrt{2}|E_{LO}|(\sin\theta)(X_\phi e^{-i\delta t}+X_\phi^*e^{i\delta t})-\sqrt{2}|E_{LO}|(X_\nu e^{-i\delta t}+X_\nu^\dagger e^{i\delta t}) , \quad \text{(A4)}$$

where, as is consistent with the pump-interaction picture, the pump phase has been taken to be zero, and the phase symmetry of the vacuum fluctuations has been employed to simplify the terms in X_ν, the vacuum-noise quadrature amplitude.

The photocurrent from the photodetector is given by

$$i(t)=\frac{1}{2}\frac{e}{\hbar\omega}\epsilon_0Ac[|E(t)|^2\eta_q-\sqrt{2}|E_{LO}|(X_\nu'e^{-i\delta t}+X_\nu'^\dagger e^{i\delta t})\sqrt{\eta_q(1-\eta_q)}] , \quad \text{(A5)}$$

where e is the electronic charge, η_q is the quantum efficiency of the detector, and A is the area of the detector. An equivalent vacuum operator X_ν' has been introduced to maintain proper fluctuation-dissipation relations.[25] The Wiener-Khintchine theorem states that the power spectral density, as displayed on a rf spectrum analyzer, of the voltage-current fluctuations of the input signal is given by[26]

$$\langle i^2(\omega)\rangle=\int_0^\infty\langle i^*(0)i(t)\rangle e^{-i\omega t}dt . \quad \text{(A6)}$$

With the help of Eq. (4) and (5), Eq. (6) tells us that the power spectral density of the photodetector output is

$$\langle i_S^2(\delta)\rangle=\left[\frac{1}{2}\frac{e}{\hbar\omega}\epsilon_0Ac\right]^2(2|E_{LO}|^2\eta_q^2\langle\sin^2\theta\rangle\langle X_\phi X_\phi^*\rangle+2|E_{LO}|^2\eta_q\langle X_\nu X_\nu^\dagger\rangle_{\mathrm{sym}}) , \quad \text{(A7)}$$

where use has been made of the fact that $\langle X_\nu X_\nu^\dagger\rangle_{\mathrm{sym}}=\langle X_\nu' X_\nu'^\dagger\rangle_{\mathrm{sym}}$. In the absence of the scattered fields, the power spectrum $\langle i_q^2(\delta)\rangle$ would contain only the beat term between the local oscillator and the vacuum fluctuations (i.e., the quantum noise). An incandescent light bulb, shined into the photodetector at an intensity such that the same dc photo-

current is obtained as during the experiment, will also produce a quantum-noise-limited signal, with spectrum $\langle i_q^2(\delta)\rangle$.[17] Spectra of incandescent light, measured independently, can be divided into the corresponding scattering spectra. The resulting ratio is given by

$$\frac{\langle i_S^2(\delta)\rangle}{\langle i_q^2(\delta)\rangle}=\frac{\langle\sin^2\theta\rangle\langle X_\phi X_\phi^*\rangle\eta_q}{\langle X_\nu X_\nu^\dagger\rangle_{\rm sym}}+1\ . \tag{A8}$$

Subtracting 1 and multiplying both sides by $\langle X_\nu X_\nu^\dagger\rangle_{\rm sym}/(\langle\sin^2\theta\rangle\eta_q)$ isolates the scattered-field power spectral density. The scattered power is also given by

$$\langle X_\phi X_\phi^\dagger\rangle=\eta_S(\delta)|E_p|^2 l=\frac{\eta_S(\delta)P_p l}{\frac{1}{2}\epsilon_0 Ac}\ , \tag{A9}$$

where $\eta_S(\delta)$ is a scattering efficiency, l is the length of the fiber, and P_p is the pump power in mks units. Then, with the help of Eq. (9), Eq. (8) can be rewritten as

$$\eta_S(\delta)=\left[\left[\frac{\langle i_s^2(\delta)\rangle}{\langle i_q^2(\delta)\rangle}-1\right]\frac{1}{l\eta_{\rm homo}\eta_q\langle\sin^2\theta\rangle P_p}\right](\tfrac{1}{2}\epsilon_0 Ac\langle X_\nu X_\nu^\dagger\rangle_{\rm sym})\ , \tag{A10}$$

where $\eta_{\rm homo}$ is a homodyne-detection efficiency which depends on the spatial overlap of the local oscillator and scattered fields, and which can be measured separately. The vacuum-noise spectral density is $(\frac{1}{2}\epsilon_0 Ac\langle X_\nu X_\nu^\dagger\rangle_{\rm sym})=\frac{1}{2}\hbar\omega(\Delta\delta/2\pi)$, where $\Delta\delta/2\pi$ is the rf bandwidth in hertz. In our publications this vacuum-noise level is defined as "1 vacuum-noise unit (VNU)."

In the case of polarized forward scattering, the scattered field is entirely in a single quadrature of the pump–local-oscillator. In this situation the phase of the local oscillator can be controlled, with the Fabry-Perot cavity shown in Fig. 6, such that θ is fixed at $\pi/2$ and we can take $\langle\sin^2\theta\rangle=1$.[17] In all other cases the phase of the scattered field relative to the local oscillator is either random, evenly distributed between quadratures, or oscillating rapidly compared to our detection bandwidth. In each of these situations we can take $\langle\sin^2\theta\rangle=\frac{1}{2}$. Thus our plots of scattered power in vacuum-noise units per milliwatt of pump power per meter of fiber length correspond to $\eta_S(\delta)$ as defined in Eq. (10). The multimode scattering $S(\omega,T)$ in Eqs. (1)–(4) in the main text is also proportional to $\eta_S(\omega)$

[1] S. Hunklinger and M. V. Schickfus, in *Amorphous Solids—Low Temperature Properties*, Vol. 24 of *Topics in Current Physics*, edited by W. A. Phillips (Springer-Verlag, Berlin, 1981), p. 81.

[2] J. C. Lasjaunias, A. Ravex, M. Vandrope, and S. Hunklinger, Solid State Commun. **17**, 1045 (1975); W. A. Phillips, Rep. Prog. Phys. **50**, 1657 (1987).

[3] U. Buchenau, H. M. Zhou, N. Nucker, K. S. Gilroy, and W. A. Phillips, Phys. Rev. Lett. **60**, 1318 (1988).

[4] P. Dutta and P. M. Horn, Rev. Mod. Phys. **53**, 497 (1981).

[5] J. Jäckle, in *Amorphous Solids—Low Temperature Properties* (Ref. 1), p. 135; N. Theodorakopoulos and J. Jäckle, Phys. Rev. B **14**, 2637 (1976).

[6] P. A. Fleury and K. B. Lyons, Phys. Rev. Lett. **36**, 1188 (1976); R. H. Stolen and M. A. Bösch, *ibid.* **48**, 805 (1982); K. B. Lyons, P. A. Fleury, R. H. Stolen, and M. A. Bösch, Phys. Rev. B **26**, 7123 (1982); J. F. Barret, J. Pelous, R. Vacher, A. K. Raychaudhuri, and M. Schmidt, J. Non-Cryst. Solids **87**, 70 (1986).

[7] C. T. Rogers and R. A. Buhrman, Phys. Rev. Lett. **55**, 859 (1985).

[8] B. Golding and J. E. Graebner, in *Amorphous Solids—Low Temperature Properties* (Ref. 1), p. 107.

[9] E. R. Grannan, M. Randeria, and J. P. Sethna, Phys. Rev. Lett. **60**, 1402 (1988).

[10] K. S. Gilroy and W. A. Phillips, Philos. Mag. B **43**, 735 (1981).

[11] G. Winterling, Phys. Rev. B **12**, 2432 (1975).

[12] S. H. Perlmutter, M. D. Levenson, R. M. Shelby, and M. B. Weissman, Phys. Rev. Lett. **61**, 1388 (1988).

[13] M. B. Weissman, Rev. Mod. Phys. **60**, 537 (1988).

[14] P. T. Thomas, N. L. Rockwell, H. M. van Driel, and G. I. Stegeman, Phys. Rev. B **19**, 4986 (1979).

[15] R. M. Shelby, M. D. Levenson, and P. W. Bayer, Phys. Rev. Lett. **54**, 939 (1985); Phys. Rev. B **31**, 5244 (1985).

[16] L. A. Firstein, J. M. Cherlow, and R. W. Hellwarth, Appl. Phys. Lett. **28**, 25 (1976).

[17] R. M. Shelby, M. D. Levenson, S. H. Perlmutter, R. G. DeVoe, and D. F. Walls, Phys. Rev. Lett. **57**, 691 (1986); R. M. Gagliard and S. Karp, *Optical Cummunication* (Wiley, New York, 1971), Chap. 5.

[18] G. J. Milburn, M. D. Levenson, R. M. Shelby, S. H. Perlmutter, R. G. DeVoe, and D. F. Walls, J. Opt. Soc. Am. B **4**, 1476 (1987); also see M. D. Levenson, in *Laser Spectroscopy and New Ideas*, Vol. 54 of *Springer Series in Optical Sciences*, edited by W. M. Yen and M. D. Levenson (Springer-Verlag, New York, 1987), p. 306.

[19] L. D. Landau and E. M. Lifshitz, *Electrodynamics of Continuous Media* (Pergamon, Oxford, 1984), p. 430; Y. S. Touloukian, R. W. Powell, C. Y. Ho, and P. G. Klemens, *Thermophysical Properties of Matter* (IFI/Plenum, New York, 1970), Vol. 2, p. 193; Y. S. Touloukian and E. H. Buyco, *Thermophysical Properties of Matter* (IFI/Plenum, New York, 1970), Vol. 5, p. 202.

[20]R. M. Waxler and G. W. Cleek, J. Res. Nat. Bur. Stand (U.S.) Sect. A **77**, 755 (1973).
[21]P. Gysel and R. K. Staubli, IEEE Photonics Tech. Lett. **PTL-1**, 327 (1989).
[22]O. L. Anderson and H. E. Bömmel, J. Am. Ceram. Soc. **38**, 125 (1955); R. Vacher and J. Pelous, Phys. Rev. B **14**, 823 (1976).
[23]R. Vacher, J. Pelous, F. Plique, and A. Zarembowitch, J. Non-Cryst. Solids **45**, 397 (1981).
[24]D. F. Walls, J. Phys. A **6**, 496 (1973).
[25]M. D. Levenson and R. M. Shelby, J. Mod. Opt. **34**, 775 (1987).
[26]N. Wiener, Acta Math. **55**, 117 (1930); A. Khintchine, Math. Ann. **104**, 604 (1934).

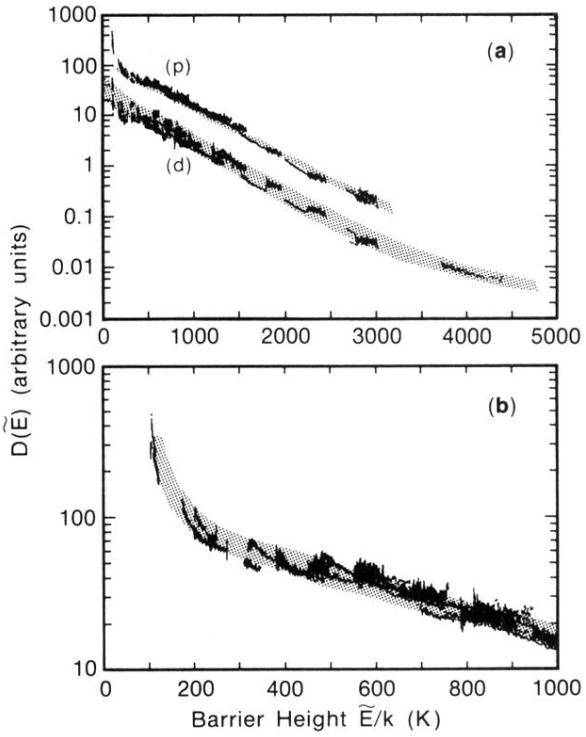

FIG. 14. (a) Experimentally inferred distribution of barrier heights of two-level systems in fused silica. The horizontal axis is in units of temperature. The individual lines correspond to polarized (p) and depolarized (d) scattering spectra like those of Fig. 7 taken at various temperatures which have been appropriately adjusted according to Eq. (6) in the text. The shaded regions represents the envelope of experimental uncertainty. The curves are well fitted by exponentials with inverse slopes of 450 K. (b) Region of the polarized $D(\tilde{E})$ curve corresponding to fiber temperatures below ~ 70 K. The constant determining the temperature scaling of the number of thermodynamically allowed thermally activated sites has been take as $\beta = 1.3$.

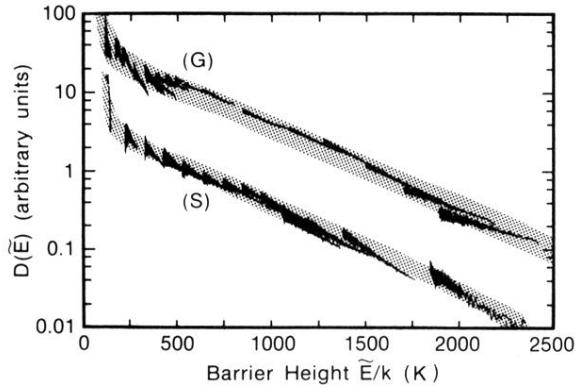

FIG. 15. $D(\tilde{E})$ for pure-fused-silica (S) and germania-doped fused-silica (G) fiber cores. Both curves are well fitted by exponentials with inverse slopes of 407 K. The constant determining the temperature scaling of the number of thermodynamically allowed thermally activated sites has been taken as $\beta = 1.3$.